SCIENTIFIC REPORTS

OPEN

SUBJECT AREAS:
ELECTRONIC PROPERTIES AND DEVICES
MECHANICAL AND STRUCTURAL PROPERTIES AND DEVICES
GRAPHENE

Received
10 December 2013

Accepted
5 February 2014

Published
26 February 2014

Correspondence and requests for materials should be addressed to H.P. (huipan@umac.mo)

Ultra-Flexibility and Unusual Electronic, Magnetic and Chemical Properties of Waved Graphenes and Nanoribbons

Hui Pan[1] & Bin Chen[2]

[1]Faculty of Science and Technology, University of Macau, Macau SAR, P. R. China, [2]Department of Engineering Mechanics, Zhejiang University, Hangzhou 310027, P. R. China.

Two-dimensional materials have attracted increasing attention because of their particular properties and potential applications in next-generation nanodevices. In this work, we investigate the physical and chemical properties of waved graphenes/nanoribbons based on first-principles calculations. We show that waved graphenes are compressible up to a strain of 50% and ultra-flexible because of the vanishing in-plane stiffness. The conductivity of waved graphenes is reduced due to charge decoupling under high compression. Our analysis of pyramidalization angles predicts that the chemistry of waved graphenes can be easily controlled by modulating local curvatures. We further demonstrate that band gaps of armchair waved graphene nanoribbons decrease with the increase of compression if they are asymmetrical in geometry, while increase if symmetrical. For waved zigzag nanoribbons, their anti-ferromagnetic states are strongly enhanced by increasing compression. The versatile functions of waved graphenes enable their applications in multi-functional nanodevices and sensors.

Graphene, a two dimensional monoatomic building block of a carbon allotrope, has attracted world-wide attention and being studied in nearly every field of science and engineering due to its exceptional charge transport, thermal, optical, and mechanical properties[1–9] and diverse potential applications[9–16]. In the electronic spectrum of pristine graphenes, valence and conduction bands cross the Fermi level at a single point in Brillouin zone (K space), the Dirac Point, and graphene is referred to as a zero band gap semiconductor or semimetal. Its particular electronic properties offer high carrier mobility and saturation velocity for future high-speed electronics. However, its semimetal nature also prevents its application in switching devices, such as logic gates and optoelectronic devices. Various methods have been introduced to open its band gap, such as functionalizing the surface, creating point/structural defects, doping other elements, and coating it on substrates[17–28]. Since ripples are difficult to avoid in two-dimensional materials and are an intrinsic feature of graphene, which strongly affect the electronic properties of graphene[29–35], controlling the rippled structures in graphene had resulted in the design of functional devices[14,29], where three dimensional (3D) periodic structures were achieved for suspended or flexible-substrate supported graphene. The ripples in graphene can accommodate large structural deformations, overcome adhesion failure under high levels of strains on flexible substrate, and allow the applications in flexible electronics. For example, the graphene with periodic ripples in one direction showed excellent flexible property[14]. Although theoretical studies showed that the ripples led to inhomogeneous charge distribution and midgap in graphene[8,36], the effects of the ripples on the elastic, electronic, magnetic, and chemical properties are absent. In this work, we investigate the physical and chemical properties of graphenes and nanoribbons with periodic ripples in one direction, called waved graphenes/nanoribbons, based on first-principles calculations. Our calculations show that waved graphenes are ultra-flexible upon compression. We also show that waved graphenes keep as semimetal, but the charge distribution is distorted. We demonstrate that their chemical reactivity is tunable by simply modulating the local curvatures. We further show that the band gap of waved armchair nanoribbon is dependent on its geometrical structure and compression, and the anti-ferromagnetic state of zigzag nanoribbon is enhanced by compression.

Results and Discussion

The waved graphene with periodic ripples along one direction, which can be experimentally achieved on a pre-strained substrate[14], is constructed by creating repeated valleys and ridges along a certain direction (see Fig. 1). In this study, we consider two kinds of waved graphenes (WGs), one with the wave along the armchair direction

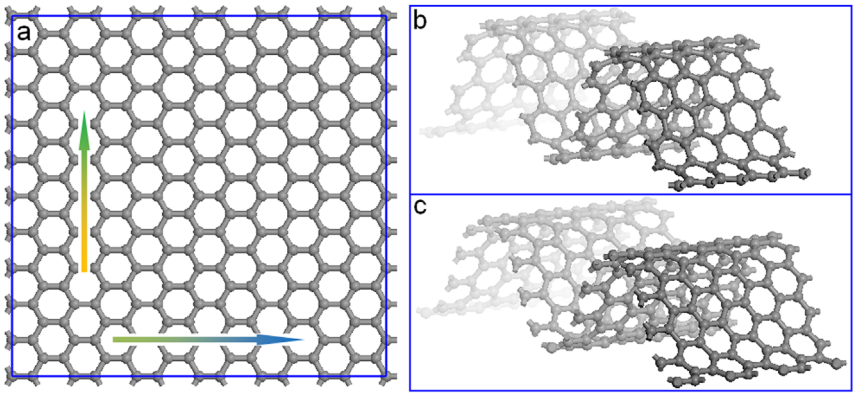

Figure 1 | Representative structures of (a) a flat graphene with arrows indicating directions of the periodic ripples, (b) a waved graphene with the periodic ripples along the armchair direction, and (c) a waved graphene with the periodic ripples along the zigzag direction.

(ac-WG) (see Fig. 1b) and another along the zigzag direction (zz-WG) (see Fig. 1c). Waved graphenes are realized based on the calculated lattice parameter of the graphene (C-C bond length is 1.427 Å). The starting wavelength of waved graphenes (c_0) is about 25 Å (referring to the supercell's length of the flat graphene along armchair/zigzag direction). Waved graphenes with shrunk wavelength (c) are realized by compression (see Fig. 2). All waved graphenes with various wavelengths are relaxed to investigate the elastic, electronic, magnetic, and chemical properties.

Ultra-flexibility. As an indication of the stability of the waved graphene, its formation energy, as compared with that of the flat graphene (FG), is calculated as:

$$E_{dif} = (E_{tot}(WG) - E_{tot}(FG))/N$$

where $E_{tot}(WG)$ is the total energy of the waved graphene under strain ($\varepsilon = \frac{c_0 - c}{c_0} \times 100\%$), $E_{tot}(FG)$ is the total energy of the flat graphene ($\varepsilon = 0$), and N is the total number of carbon atoms in the supercell. The calculated energy difference (E_{dif}) between the waved and flat graphenes shows that the energy of the waved graphene linearly increases with the compression (the reduction of wavelength) (see Figs. 3a&d). The increment of the energy is only 1.5% per atom with a compression up to 50% (see inset in Fig. 3a). If the graphene keeps flat under the compression, its energy goes nonlinearly up with increasing strain (see Fig. 3b and inset in Fig. 3d). By comparing the energy of the waved graphene with that of the flat one under the same strain, we see that the energy increment in both of them are almost equal when $\varepsilon \leq 1\%$ (see Fig. 3c). When $\varepsilon > 1$, the energy of the waved graphene is much less than that of the flat one (see Fig. 3), indicating that the graphene cannot keep flat under high compression ($\varepsilon > 1\%$). Our calculations confirm that the waved graphene is stable because the slope of energy increment is very low (~2.63 and 2.96 meV/atom for ac-WG and zz-WG, respectively) (see Figs. 3a&d), and can be easily obtained on a pre-strained substrate[14].

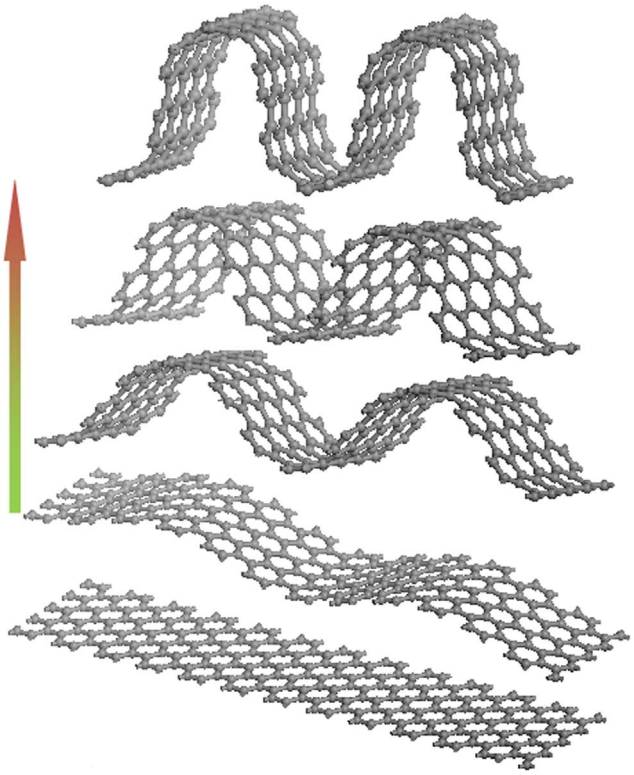

Figure 2 | **Representative structures of flat and waved graphenes with various wavelengths.**

The strain energy ($E_S(\varepsilon)$), namely, the total energy at a given strain ε minus the total energy at zero strain, is given by $E_{dif} \times N$. Then, we can obtain the tension force ($F_T = -\partial E_S(\varepsilon)/\partial c$), the force constant ($\kappa = \partial^2 E_S(\varepsilon)/\partial c^2$), and the in-plane stiffness ($C = \frac{1}{A_0}\partial^2 E_S(\varepsilon)/\partial \varepsilon^2$) in terms of the equilibrium area of the supercell (A_0)[37–39]. The calculated tension forces are 0.24 and 0.41 eV/Å for ac-WG and zz-WG, respectively. Because of the linear relationship between the strain energy and the compression, the force constant and in-plane stiffness of the waved graphene are zero, indicating that they are ultra-flexible and keep undamaged even the substrate is released from high pre-strain, which is consistent with the experimental results in literatures [14]. The ultra-flexibility of waved graphenes enables their applications in stretchable devices.

Electronic properties of waved graphenes. Similar to the lattice structure of waved graphenes that keeps stable under compression, the band structures of waved graphenes are not strongly affected. For the waved graphene with its ripples along the armchair direction (ac-WG), the calculated band structures are almost unaffected by the applied compression up to 50% (or the reduction of wavelength) (see Fig. 4). We clearly see that the Dirac cone of flat graphene is at around 1/3 along the reciprocal direction M (0, 0.5, 0) to Γ (0, 0, 0) (see Fig. 4a), which is almost unchanged with the increasing compression (see Figs. 4b ~ f). We also note that more states in the conduction band are pushed down with the increasing compression (see Fig. 4). Similar to the response of ac-WGs to external strains, the graphene with its ripples along the zigzag direction (zz-WG) is also tolerant to the compression (or the reduction of wavelength). The calculated

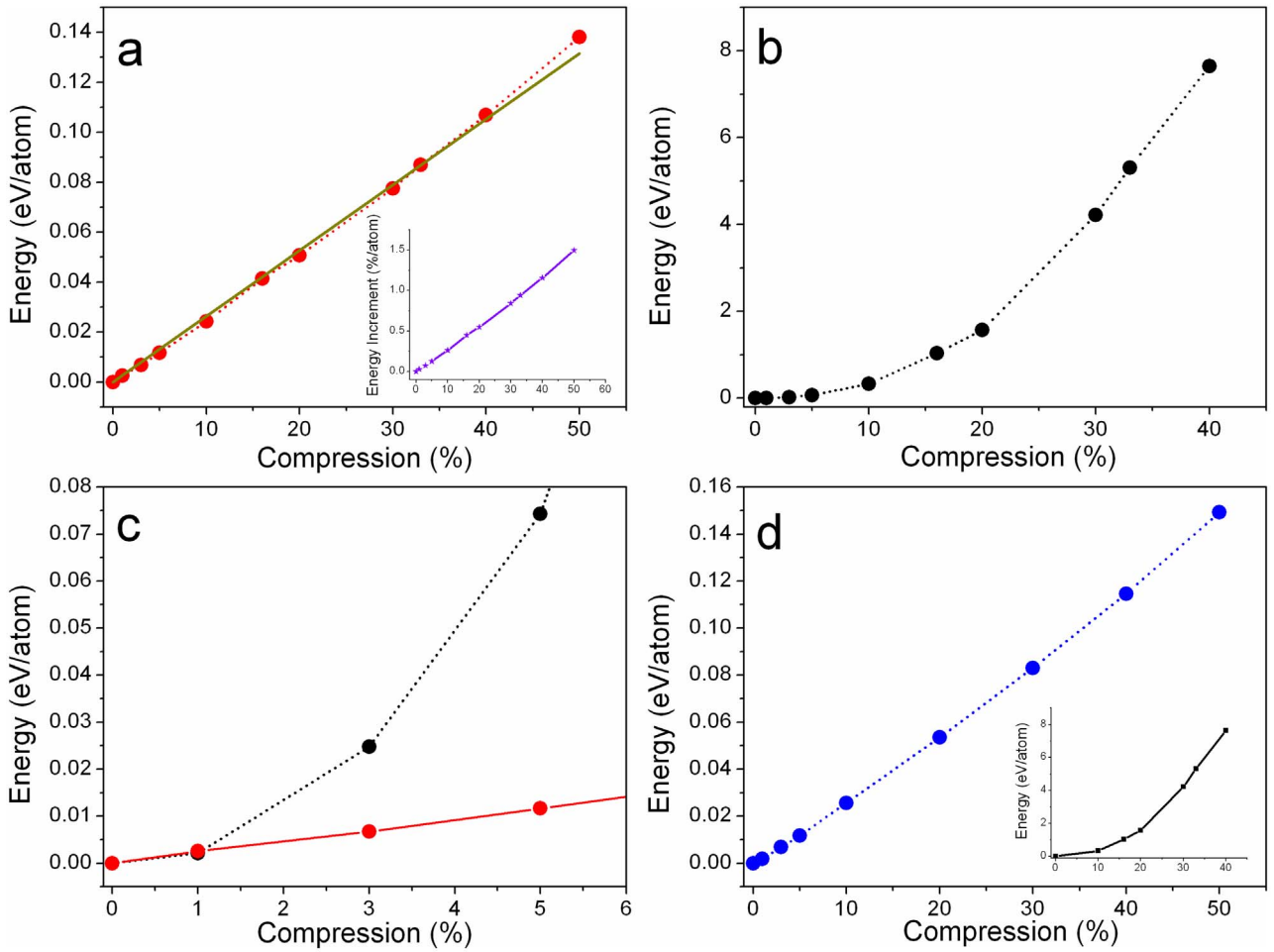

Figure 3 | The calculated strain energies of ac-WG (a) and flat graphene (b) as a function of compression along the armchair direction. (c) fine-view comparison of the calculated strain energies of ac-WG and flat graphene with a compression up to 6%. (d) The calculated strain energies of zz-WG as a function of compression along the zigzag direction. Inset in (a) is the incremental energy as a function of compression. Inset in (d) is the calculated strain energies of flat graphene as a function of compression along the zigzag direction.

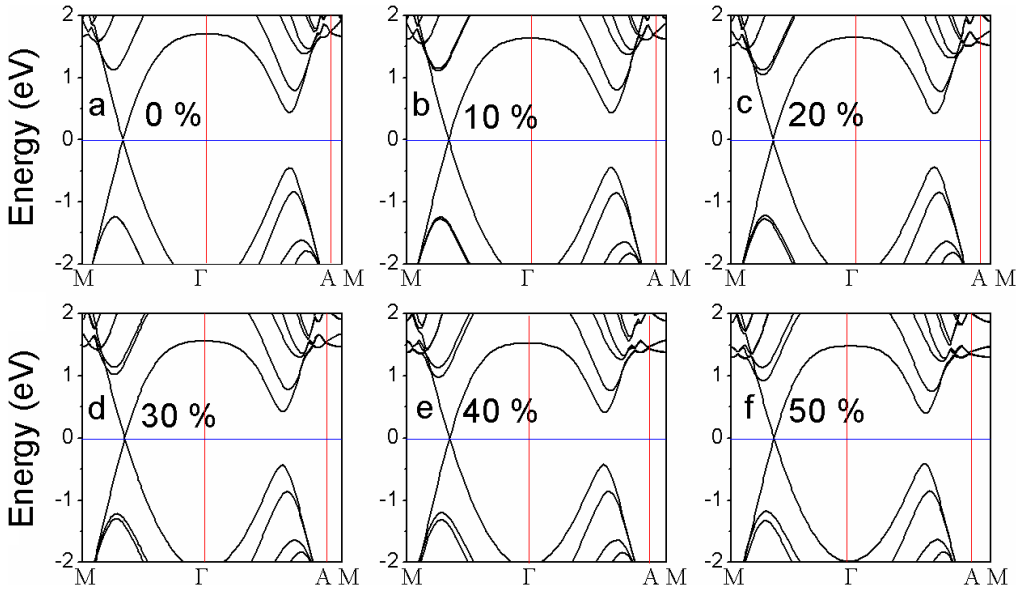

Figure 4 | **The calculated band structures of ac-WGs under different compressions.** The Fermi level is at 0 eV.

band structures show that the Dirac cone keeps almost unchanged with the increase of compression (see Fig. 5), indicating they are semi-metallic. The band structure also keeps unaffected under the compression, except the Dirac cones near the Fermi level under high compression, which are distorted with energy levels being pushed down and flattened within the reciprocal region (M to Γ) (see Figs. 5e&f). The calculated electronic structures of wave graphenes show that their conducting characters are unaffected by the compression. To further reveal the effects of compression on the conductivity, the charge densities of bands near the Fermi level, including conduction band bottom (CBB) and valence band top (VBT), are calculated. It is well-known that the VBT and CBB states of the flat graphene are attributed to the big π bonding and anti-bonding (π*) states[8,9]. Similar to flat graphene, the big π and π* states of the zz-WG keep extended in the whole structure (see Fig. 6). The bending in the zz-WG occurs at the shared length between two hexagons (see inset in Fig. 6), which may not destroy the coupling between the big π bonding states of zz-WG under lower compression. However, the coupling is distorted by high compression (see Fig. 5), leading to the distortion of Dirac cone. Different from zz-WG, the bending in the ac-WG occurs at the bridge between two hexagons (see inset in Fig. 7), which could result in the decoupling between the big π bonding states in the neighboring hexagons. As shown in the calculated charge densities of VBT and CBB of the ac-WG, the coupling between π bonding states along the wave is weakened due to the curvature (see Fig. 7a). The decoupling between π bonding states in valence band leads to the charge redistribution, which confirms the reduction of conductivity[8]. We see that the weak compression may have less effect on the conductivity of zz-WG, while the resistance of ac-WGs should increase. It is expected that the waved graphenes can be mechanical sensors and the change of resistance can also indicate the orientation of periodic ripples on graphene.

Chemistry of waved graphenes. The ripples in waved graphenes affect not only their conducting properties, but their chemistry as well, due to local curvatures. According to the "π-orbital axis vector" (POAV) theory[40–44], carbon atoms at edges, defects, or regions of high local curvature are more active due to the elevated chemical potential and strain energy, while the carbon atoms at flat regions are relatively inert due to conjugation[40–49]. The heightened chemical reactivity of atoms at those sites with local conformational deformation can be quantitatively characterized by the POAV pyramidalization angle[40–44], which is defined as $(\theta_{\sigma\pi} - 90^\circ)$ with $\theta_{\sigma\pi}$ being the common angle made by the π-orbital axis vector and the σ bonds[43,50,51]. The calculated POAV angles of the atoms on the waved graphenes (see Fig. 8) show that the chemical reactivity of carbon atom depends on its location and the current wavelength (or compression) as well. The plot of POAV angles of the atoms on a waved graphene (see Fig. 2) appears to follow a similar wave shape as that of the graphene, which is different from these in a fullerene (POAV angle in C_{60} is 11.64°)[43] and a single-walled carbon nanotube (for example, 5.15° in zigzag (10, 0) SWCNT)[49]. The $\theta_{\sigma\pi}$ at crest and trough deviates significantly from 90°, with larger POAV angles at crest (positive) and trough (negative), indicating the high chemical reactivity at these sites due to the high strain energy (see Fig. 8). The POAV angle (negative) increases as the location of an atom shifts from the trough to the middle between trough and crest, which is due to the release of curvature, indicating the gradual reduction of the chemical

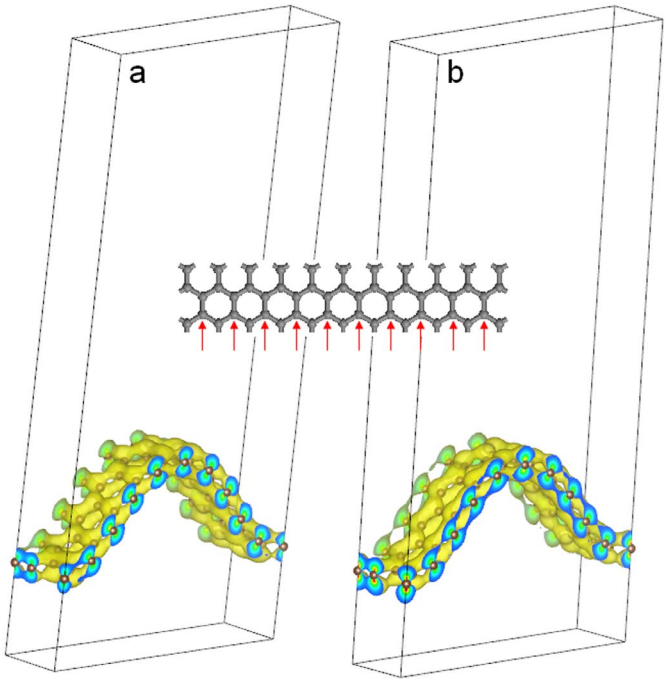

Figure 6 | The calculated charge densities of (a) valence band top and (b) conduction band bottom of zz-WG under a compression of 20%. The inset shows the flat graphene with arrows indicating the bending of zz-WG that occurs.

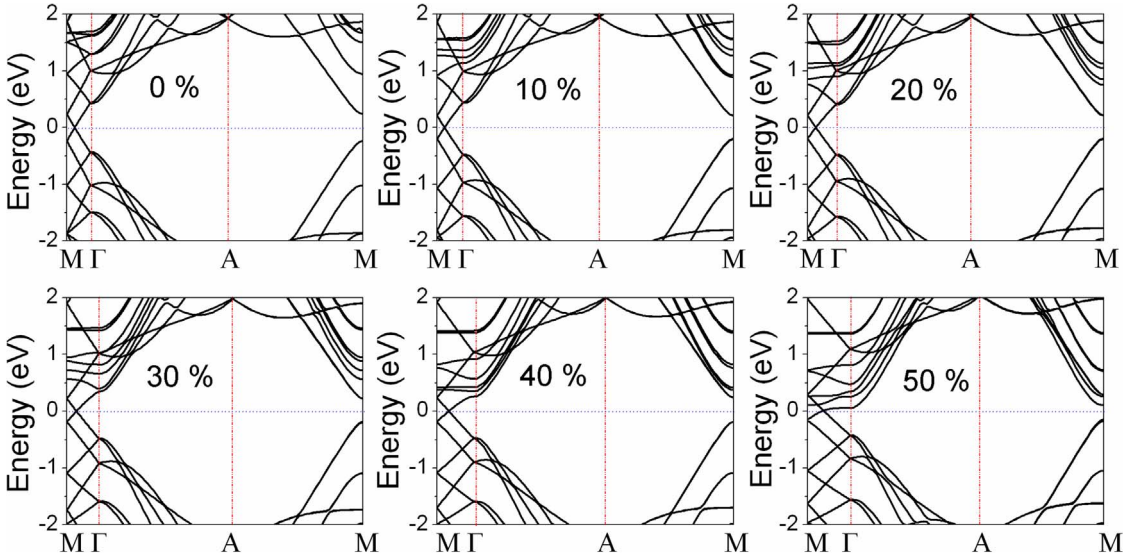

Figure 5 | **The calculated band structures of zz-WGs under different compressions.** The Fermi level is at 0 eV.

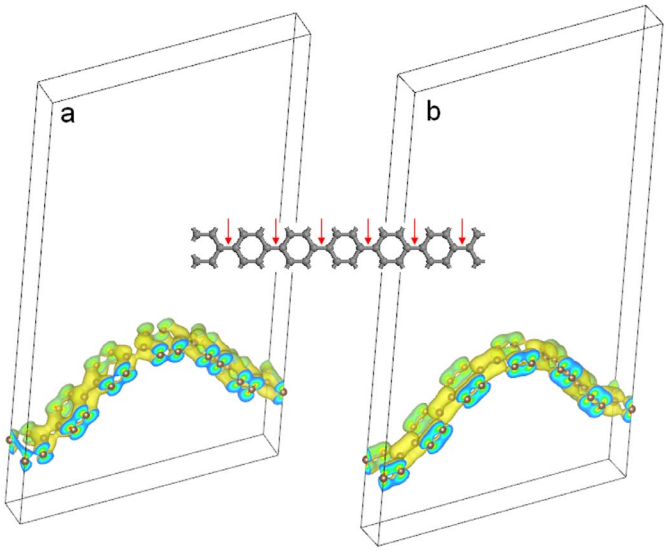

Figure 7 | The calculated charge densities of (a) valence band top and (b) conduction band bottom of ac-WG under a compression of 20%. The inset shows a flat graphene with arrows indicating the bending of ac-WG that occurs.

reactivity. With its location further shifting from the middle between the trough and the crest to the crest, the POAV angle (positive) continue to increase and the chemical reactivity is therefore further enhanced. Notably, the POAV angles of atoms at crest (positive) increase and those at the trough (negative) decrease with the reduction of the wavelength or the increment of compression because of the increased local curvature (see Fig. 8), suggesting that the chemical reactivity can be enhanced by compressing the waved graphene. Considering its ultra-flexibility, the chemical reactivity of carbon atoms on waved graphene can be easily controlled and the chemical reaction on waved graphene can be modulated by a simple mechanical compression or stretch. The waved graphenes may possess the similar chemistry of molecular species as those of SWNCT and fullerene with improved and controllable reactivity.

Electronic and magnetic properties of waved graphene nanoribbons. Different from the stable lattice and tolerant band structure of waved graphenes under compression, the electronic properties of waved nanoribbons are evidently affected by applied strains. To construct nanoribbons, the chirality and symmetry are considered, including armchair and zigzag nanoribbons with asymmetrical and symmetrical edges, respectively (see Supplementary Figs. S1 online). Waved graphene nanoribbons (WG-NR) under the compression from 10 to 50% are directly built from the optimized structures of the waved graphenes under the same compression, and their edge dangling states are saturated by H atoms.

For convenience, we adopt the parameter (p) to define the width of armchair WG-NRs, which is equal to the number of carbon dimer lines in the super cell (see Supplementary Figs. S1a & S1b online). Our calculations show that armchair WG-NRs (ac-WG-NRs) are direct band semiconductors and non-magnetic (see Fig. 9). The calculated band structures show that the band gaps of ac-WG-NRs with asymmetrical edges ($p = 16$) are larger than those with symmetrical edges ($p = 17$) (see Figs. 9a&g) under vanishing compression, because the band gap of graphene nanoribbons exhibits three distinct families of characteristic behaviours with width (p) and the gap hierarchy follows $E_{g,\,3n+1} > E_{g,\,3n} > E_{g,\,3n+2}$ (where n is a positive integer, and $p = 3n + m$ ($m = 0$, 1, or 2))[39,52]. Interestingly, the band gap of asymmetrical ac-WG-NR (ac-WG-NR-a) increases at first with the compression up to 10% (see Figs. 9a&b), and then reduces with the further increment of the compression (see Figs. 9c ~ f). The change of band gap as a function of compression is shown in Fig. 10. Clearly, we see that conduction band bottom (CBB) and valence band top (VBT) move up and down, respectively, within the compression from 0 to 10% (see Fig. 9b), resulting in the increment of band gap. We also note that the energy level just above CBB (CBB-a) and that below VBT (VBT-b) move reversely to the movement of CBB and VBT under the compression. At 10% compression, the CBB and CBB-a, and VBT and VBT-b join together at Γ points, leading to the maximal band gap of ac-WG-NR-a. By further increasing the compression, CBB-a becomes new CBB and moves down, VBT-b becomes new VBT and moves up, resulting in the reduction of the band gap of ac-WG-NR-a (see Figs. 9c ~ f). Different from ac-WG-NR-a, the calculated band structures show that the band gap of symmetrical ac-WG-NR (ac-WG-NR-s) increases linearly with the increment of compression (see Figs. 9g ~ m & Fig. 10). We also see that its CBB and VBT move up and down as the compression increases, respectively, leading to the increment of band gap under compression. Although CBB-a and VBT-b also move oppositely to the movements of CBB and VBT, the gap spaces between CBB and CBB-a, and VBT and VBT-b are too large for CBB-a and VBT-b to overtake CBB and VBT (see Figs. 9g ~ m). The charge density of each energy band further confirms the movement of these bands under compression (see Supplementary Figs. S2 & S3 online).

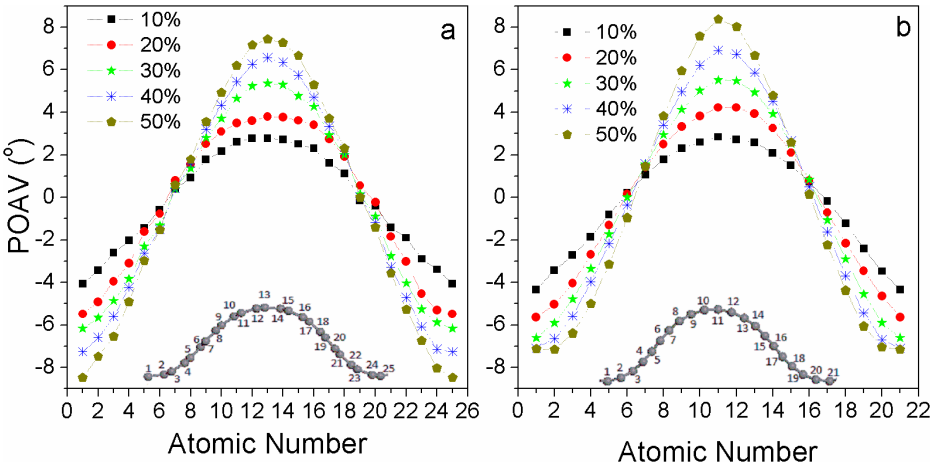

Figure 8 | The calculated pyramidalization angles of carbon atoms within one wavelength of waved graphene with the ripples along (a) the armchair direction (ac-WG) and (b) the zigzag direction (zz-WG) under compression (10 ~ 50%). The insets indicate the locations of carbon atoms in ac-WG and zz-WG under a compression of 20%, for example.

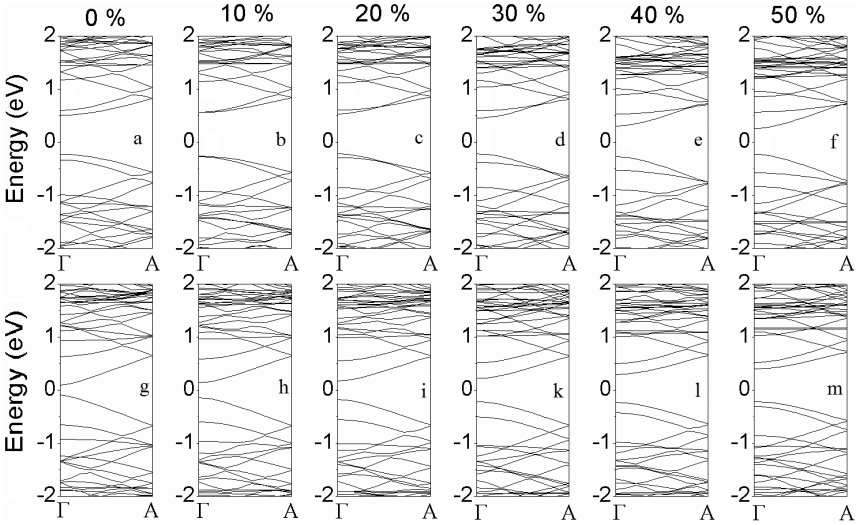

Figure 9 | The calculated band structures of armchair waved graphene nanoribbons with asymmetrical edges (up row) and symmetrical edges (down row) under compressions. The Fermi level is at 0 eV.

Previous theoretical studies showed that the zigzag graphene nanoribbons exhibit an antiferromagnetic insulating ground state with edge-state electrons that experience ferromagnetic coupling at each edge but antiferromagnetic coupling across the ribbon[52–54]. Our calculated exchange energies (energy difference between anti-ferromagnetic and ferromagnetic states, $E_{afm} - E_{fm}$) also show that the zigzag graphene nanoribbons without compression are anti-ferromagnetic because that the energies of anti-ferromagnetic states are lower than those of ferromagnetic states. At the same time, we find that the anti-ferromagnetic ground state of asymmetrical nanoribbon is more stable than that of symmetrical one because of the relatively higher exchange energy (see Fig. 11). Most importantly, we see that the anti-ferromagnetic ground states of zigzag waved graphene nanoribbons (zz-WG-NRs) are efficiently enhanced by applying compression (or the reduction of the wavelength) (see Fig. 11). The exchange energies of asymmetrical and symmetrical zz-WG-NRs (zz-WG-NR-a and zz-WG-NR-s) are increased by 50% and 65%, respectively, under a compression up to 50%. The calculated band structures of zz-WG-NRs show that they are semiconductors with band gaps of ~0.4 eV (see Supplementary Fig. S4 online). The calculated band structures of zigzag graphene nanoribbons without compression are consistent with the literatures[52,53], but their band gaps are less than those in Ref. 53 because the quasi-particle effect is not considered in this work. Their band gaps are almost unaffected by the compression, except under high compression of 50%, which leads to the change from direct band to indirect band and the reduction of band gap (~15%) (see Supplementary Fig. S4 online).

The dependence of compression of the electronic and magnetic properties of WG-NRs demonstrates that they are sensitive to applied strain and may be applicable to a variety of functional nanodevices. For example, ac-WG-NRs can be used as mechanical switches and sensors, and electronic devices with adjustable threshold voltage because their band gaps can be easily controlled by compression. By engineering their edge structures and applying strains, multi-functional nanodevices may be achievable because their band structures as a function of compression are also edge-dependent. Similarly, the magnetic response of zz-WG-NRs to applied compression also indicates that they can be used in mechanical sensors and spintronics. Reversely, the edge structures of WG-NRs can be easily characterized by measuring their responses to compression in experiments.

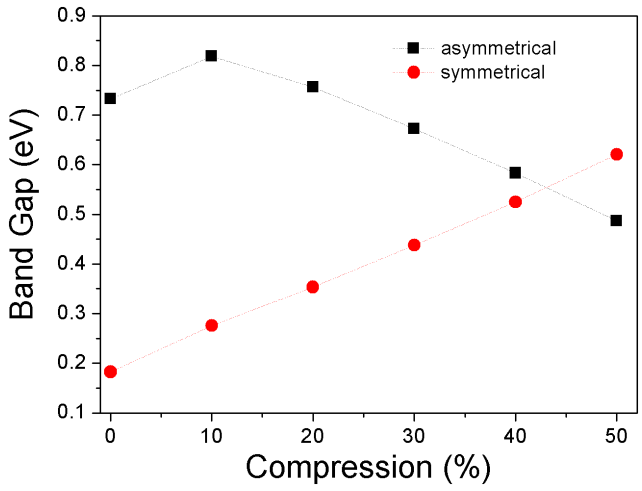

Figure 10 | The calculated band gap of armchair waved graphene nanoribbons with asymmetrical edges and symmetrical edges as a function of compression.

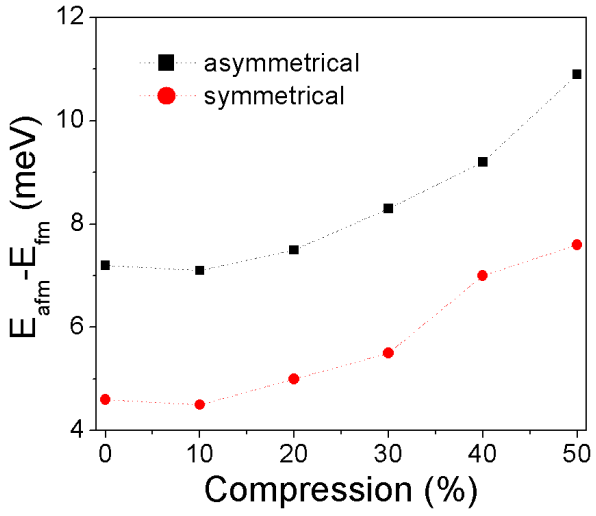

Figure 11 | The calculated exchange energies of zigzag waved graphene nanoribbons with asymmetrical edges and symmetrical edges as a function of compression.

Conclusions

In summary, we present a first-principles study on the elastic, electronic, magnetic, and chemical properties of waved graphenes and nanoribbons. We find that waved graphenes show ultra-flexiblility and are compressible up to 50% with a starting wavelength of ~25 Å, which can be higher with a larger starting wavelength. We show that the conductivity of waved graphenes depends on the chirality of the periodic ripples. Waved graphenes with periodic ripples along the armchair direction show increased resistance under applied compression due to the decoupling between the π bonding states in valence band. The characteristics of the band structure of graphene, such as Dirac point, keep unaffected with the existence of periodic ripples, except waved graphenes with periodic ripples along zigzag direction under a compression of 50%, where the Dirac point is distorted. We predict that the chemical reactivity of waved graphene can be easily modulated by applying external stain to tune its wavelength or local curvature. The band gaps of armchair waved graphene nanoribbons can be controlled and the anti-ferromagnetic ground stated of zigzag waved graphene nanoribbons are greatly enhanced by the applied compression. Waved graphenes and nanoribbons may find applications in stretchable nanodevices, mechanical sensors and switches, chemical reaction, and spintronics by controlling external strains and engineering edge structures. Our calculations also suggest a simple approach to determine the edge structures of nanoribbons by detecting their electronic and magnetic response, and chemical reactivity to applied strains.

Methods

The first-principles calculations based on the density functional theory (DFT)[55] and the Perdew-Burke-Eznerhof generalized gradient approximation (PBE-GGA)[56] are carried out to study the electronic and elastic properties of waved graphenes. The projector augmented wave (PAW) scheme[57,58] as incorporated in the Vienna ab initio simulation package (VASP)[59] is used in the study. The Monkhorst and Pack scheme of k point sampling is used for integration over the first Brillouin zone[60]. A $15 \times 1 \times 1$ grid for k-point sampling for geometry optimization and calculations of density of states, respectively, and an energy cut-off of 500 eV are consistently used for the nanoribbons in our calculations. Good convergence is obtained with these parameters and the total energy was converged to 2.0×10^{-5} eV/atom.

1. Novoselov, K. S. *et al*. Electric field effect in atomically thin carbon films. *Science* **306**, 666–669 (2004).
2. Novoselov, K. S. *et al*. Two-dimensional gas of massless Dirac fermions in graphene. *Nature* **438**, 197–200 (2005).
3. Du, X., Skachko, I., Duerr, F., Luican, A. & Andrei, E. Y. Fractional quantum Hall effect and insulating phase of Dirac electrons in graphene. *Nature* **462**, 192–195 (2009).
4. Han, M. Y., Ozyilmaz, B., Zhang, Y. & Kim, P. Energy band-gap engineering of graphene nanoribbons. *Phys. Rev. Lett.* **98**, 206805 (2007).
5. Zhang, Y. B., Tan, Y. W., Stormer, H. L. & Kim, P. Experimental observation of the quantum Hall effect and Berry's phase in graphene. *Nature* **438**, 201–204 (2005).
6. Novoselov, K. S. *et al*. Room-temperature quantum Hall effect in graphene. *Science* **315**, 1379 (2007).
7. Lee, C., Wei, X., Kysar, J. W. & Hone, J. Measurement of the elastic properties and intrinsic strength of monolayer graphene. *Science* **321**, 385–388 (2008).
8. Castro Neto, A. H., Guinea, F., Peres, N. M. R., Novoselov, K. S. & Geim, A. K. The electronic properties of graphene. *Rev. Mod. Phys.* **81**, 106–162 (2009).
9. Das Sarma, S., Adam, S., Gwang, E. H. & Rossi, E. Electronic transport in two-dimensional graphene. *Rev. Mod. Phys.* **83**, 407–470 (2011).
10. Bao, X L. & Loh, K. P. Graphene photonics, plasmonics, and broadband optoelectronics devices. *ACS Nano* **6**, 3677–3694 (2012).
11. Loh, O. Y. & Espinosa, H. D. Nanoelectromechanical contact switches. *Nature Nanotechnol.* **7**, 283–295 (2012).
12. Zhao, X., Hayner, C. M., Kung, M. C. & Kung, H. H. Flexible holey graphene paper electrodes with enhanced rate capability for energy storage applications. *ACS Nano* **5**, 8739–8749 (2011).
13. Koester, S. J. & Li, M. High-speed waveguide-coupled graphene-on-graphene optical modulators. *Appl. Phys. Lett.* **100**, 171107 (2012).
14. Wang, Y. *et al*. Super-elastic graphene ripples for flexible strain sensors. *ACS Nano* **5**, 3645–3650 (2011).
15. Bellido, E. P. & Seminario, J. M. Graphene-based vibronic devices. *J. Phys. Chem. C* **116**, 8409–8416 (2012).
16. Lu, Y. *et al*. Graphene-protein bioelectronic devices with wavelength-dependent photoresponse. *Appl. Phys. Lett.* **100**, 033110 (2012).
17. Lehtinen, P. O., Foster, A. S., Ayuela, A., Krasheninnikov, A., Nordlund, K. *et al*. Magnetic properties and diffusion of adatoms on a graphene sheet. *Phys. Rev. Lett.* **91**, 017202 (2003).
18. Zhou, J. *et al*. Ferromagnetism in semihydrogenated graphene sheet. *Nano. Lett.* **9**, 3867–3870 (2009).
19. Pereira, V. M., Guinea, F., Lopes dos Santos, J. M. B., Peres, N. M. R. &Neto, A. H. C. Disorder induced localized states in graphene. *Phys. Rev. Lett.* **96**, 036801 (2006).
20. Gass, M. H. *et al*. Free-standing graphene at atomic resolution. *Nat. Nanotechnol.* **3**, 676–681 (2008).
21. Banhart, F., Kotakoski, J. & Krasheninnikov, A. V. Structural defects in grapheme. *ACS Nano* **5**, 26–41 (2011).
22. Casolo, S., Martinazzo, R. & Tantardini, G. F. Band engineering in graphene with superlattices of substitutional defects. *J. Phys. Chem. C* **115**, 3250–3256 (2011).
23. Lee, S. H. *et al*. Band gap opening by two-dimensional manifestation of Peierls instability in graphene. *ACS Nano* **5**, 2964–2969 (2011).
24. Suggs, K., Reuven, D. & Wang, X. Q. Electronic properties of cycloaddition-functionalized graphene. *J. Phys. Chem. C* **115**, 3313–3317 (2011).
25. Abanin, D. A., Shytov, A. V. & Levitov, L. S. Peierls-type instability and tunable band gap in functionalized graphene. *Phys. Rev. Lett.* **105**, 086802 (2010).
26. Singh, A. K., Penev, E. S. & Yakobson, B. I. Vacancy clusters in graphane as quantum dots. *ACS Nano* **4**, 3510–3514 (2010).
27. Naumov, I. I. & Bratkovsky, A. M. Gap opening in graphene by simple periodic inhomogeneous strain. *Phys. Rev. B* **84**, 245444 (2011).
28. Hong, J. M. *et al*. Room-temperature magnetic ordering in functionalized grapheme. *Sci. Rep.* **2**, 624 (2012).
29. Bao, W. Z. *et al*. Controlled ripple texturing of suspended graphene and ultrathin graphite membranes. *Nature Nanotechnol.* **4**, 562–566 (2009).
30. Meyer, J. C. *et al*. The structure of suspended graphene sheets. *Nature* **446**, 60–63 (2007).
31. N'Diaye, A. T., Bliekamp, S., Feibelman, P. J. & Michely, T. Two-dimensional Ir cluster lattice on a graphene Moiré on Ir(111). *Phys. Rev. Lett.* **97**, 215501 (2006).
32. Zhang, L., Zeng, X. & Wang, X. Programmable hydrogenation of graphene for novel nanocages. *Sci. Rep.* **3**, 3162; DOI:10.1038/srep03162 (2013).
33. Paronyan, T. M., Pigos, E. M., Chen, G. G. & Harutyunyan, A. R. Formation of ripples in graphene as a result of interfacial instabilities. *ACS Nano* **5**, 9619–9627 (2011).
34. de Juan, F., Cortijo, A., Vozmediano, M. A. H. & Cano, A. Aharonov-Bohm interferences from local deformations in graphene. *Nature Phys.* **7**, 810–815 (2011).
35. Fan, X. Y., Nouchi, R. & Tanigaki, K. Effect of charge puddles and ripples on the chemical reactivity of single layer graphene supported by SiO_2/Si substrate. *J. Phys. Chem. C* **115**, 12960–12964 (2011).
36. Guinea, F., Katsnelson, M. I. & Vozmediano, M. A. H. Midgap states and charge inhomogeneities in corrugated graphene. *Phys. Rev. B* **77**, 075422 (2008).
37. Yakobson, B., Brabec, C. & Bernholc, J. Nanomechanics of carbon tubes: Instabilities beyond linear response. *Phys. Rev. Lett.* **76**, 2511–2514 (1996).
38. Ataca, C., S-ahin, H., Akt€urk, E. & Ciraci, S. Mechanical and electronic properties of MoS_2 nanoribbons and their defects. *J. Phys. Chem. C* **115**, 3934–3941 (2011).
39. Shi, H. L., Pan, H., Zhang, Y. W. & Yakoboson, B. I. Electronic and magnetic properties of graphene-fluorographene superlattices. *J. Phys. Chem. C* **116**, 18278–18283 (2013).
40. Haddon, R. C. Hybridization and the orientation and alignment of π-orbitals in nonplanar conjugated organic molecules: π-orbitals axis vector analysis (POAV2). *J. Am. Chem. Soc.* **108**, 2837–2842 (1986).
41. Haddon, R. C. Rehybridization and π-orbital overlap in nonplanar conjugated organic molecules: π-orbitals axis vector (POAV) analysis and three-dimensional Huckel molecular orbital (3D-HMO) theory. *J. Am. Chem. Soc.* **109**, 1676–1685 (1987).
42. Haddon, R. C. Pyramidalization: geometrical interpretation of the π -orbital axis vector in three dimensions. *J. Phys. Chem.* **91**, 3719–3720 (1987).
43. Haddon, R. C. Chemistry of the fullerenes: The manifestation of strain in a class of continuous aromatic molecules. *Science* **261**, 1545–1550 (1993).
44. Haddon, R. C. Measure of nonplanarity in conjugated organic molecules: Which structurally characterized molecule displays the highest degree of pyramidalization? *J. Am. Chem. Soc.* **112**, 3385–3389 (1990).
45. Wu, Q. Z. *et al*. Selective surface functionalization at regions of high local curvature in graphene. *ChemComm* **49**, 677–679 (2013).
46. Srivastava, D. *et al*. Predictions of enhanced chemical reactivity at regions of local conformational strain on carbon nanotubes: kinky chemistry. *J. Phys. Chem. B* **103**, 4330–4337 (1999).
47. Han, J. & Jaffe, R. Energetics and geometries of carbon nanoconic tips. *J. Chem. Phys.* **108**, 2817–2823 (1998).
48. Bekyarova, E. *et al*. Effect of covalent chemistry on the electronic structure and properties of carbon nanotube and graphene. *Acc. Chem. Res.* **46**, 65–76 (2013).
49. Niyogi, S. *et al*. Chemistry of single-walled carbon nanotubes. *Acc. Chem. Res.* **35**, 1105–1113 (2002).
50. Weedon, B. R., Haddon, R. C., Spielmann, H. P. & Meier, M. S. Fulleroid addition regiochemistry is driven by π-orbital misalignment. *J. Am. Chem. Soc.* **121**, 335–340 (1999).

51. Haddon, R. C. Comment on the relationship of the pyramidalization angle at a conjugated carbon atom to the σ bond angles. *J. Phys. Chem. A* **105**, 4164–4165 (1993).
52. Son, Y. W., Cohen, M. & Louie, S. Energy gaps in graphene nanoribbons. *Phys. Rev. Lett.* **97**, 216803 (2006).
53. Son, Y. W., Cohen, M. L. & Louie, S. G. Half-metallic graphene nanoribbons. *Nature* **444**, 347–349 (2006).
54. Li, Y., Cohen, M. L. & Louie, S. G. Magnetic edge-state excitons in zigzag graphene nanoribbons. *Phys. Rev. Lett.* **101**, 186401 (2008).
55. Hohenberg, P. & Kohn, W. Inhomogeneous electron gas. *Phys. Rev.* **136**, B864–B871 (1964).
56. Blöchl, P. E. Projector augmented-wave method. *Phys. Rev. B* **50**, 17953–17979 (1994).
57. Perdew, J. P., Burke, K. & Ernzerhof, M. Generalized gradient approximation made simple. *Phys. Rev. Lett.* **77**, 3865–3868 (1996).
58. Kresse, G. & Joubert, D. From ultrasoft pseudopotentials to the projector augmented-wave method. *Phys. Rev. B* **59**, 1758–1775 (1999).
59. Kresse, G. & Furthmuller, J. Efficient iterative schemes for ab initio total-energy calculations using a plane-wave basis set. *Phys. Rev. B* **54**, 11169–11186 (1996).
60. Monkhorst, H. J. & Pack, J. Special points for brillouin-zone integrations. *Phys. Rev. B* **13**, 5188–5192 (1976).

Acknowledgments

Hui Pan thanks the support of Start-up Research Grant (SRG-2013-00033-FST) at University of Macau. The DFT calculations were performed at High Performance Computing Cluster (HPCC) of Information and Communication Technology Office (ICTO) at University of Macau.

Author contributions

H.P. proposed the idea, performed the calculations, and wrote the paper. B.C. contributed to analysis of results. All authors reviewed the manuscript.

Additional information

Supplementary information accompanies this paper at http://www.nature.com/scientificreports

Competing financial interests: The authors declare no competing financial interests.

How to cite this article: Pan, H. & Chen, B. Ultra-Flexibility and Unusual Electronic, Magnetic and Chemical Properties of Waved Graphenes and Nanoribbons. *Sci. Rep.* **4**, 4198; DOI:10.1038/srep04198 (2014).